THE JOURNAL OF PHYSICAL CHEMISTRY C

ARTICLE

pubs.acs.org/JPCC

Photoinduced Charge Transfer and Polaron Dynamics in Polymer and Hybrid Photovoltaic Thin Films: Organic vs Inorganic Acceptors

Kevin M. Noone,[†] Selvam Subramaniyan,[‡] Qifeng Zhang,[§] Guozhong Cao,[§] Samson A. Jenekhe,[‡] and David S. Ginger*[,†]

[†]Department of Chemistry, [‡]Department of Chemical Engineering, and [§]Department of Materials Science and Engineeering, University of Washington, Seattle, Washington 98195, United States

Supporting Information

ABSTRACT: We use photoinduced absorption (PIA) spectroscopy to study charge generation and recombination in a series of bulk heterojunction blends relevant to organic and hybrid solar cells. We compare both organic and inorganic electron acceptors, including the fullerene, phenyl-C_{61}-butyric acid methyl ester (PCBM), oxides such as ZnO and TiO_2, and colloidal quantum dots, including CdSe and PbS nanocrystals. We use a variety of donor host polymers, including poly(3-hexylthiophene) (P3HT), poly[2-methoxy-5-(3′,7′-dimethyl-octyloxy)-*p*-phenylenevinylene] (MDMO-PPV), and poly(2,3-bis(2-hexyldecyl)quinoxaline-5,8-diyl-*alt*-*N*-(2-hexyldecyl)-dithieno-[3,2-*b*:2′,3′-*d*]pyrrole) (PDTPQx-HD). In every case, we measure longer average carrier lifetimes in blends with the inorganic acceptors as compared to blends with PCBM. The PIA data also suggest that the internal electric fields are attenuated in the inorganic blends, consistent with increased screening between the photogenerated carriers due to the higher dielectric constants of the inorganic nanoparticles. Using ligand exchange experiments, we further demonstrate that surface electron trapping on the inorganic colloids contributes to at least part of the increased lifetime in the PDTPQx-HD/PbS blends and that ligand exchange to remove traps can be used to improve the performance of these polymer/low-band-gap quantum dot hybrid photovoltaics.

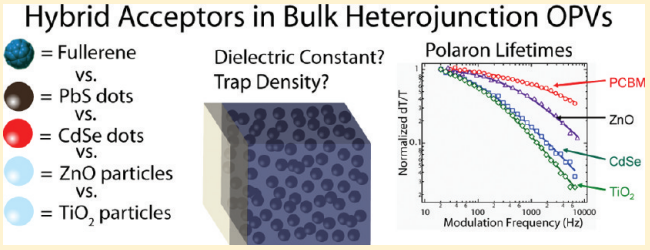

INTRODUCTION

Organic photovoltaics (OPVs) can be manufactured using low-cost, high-throughput printing, making them candidates for large-scale solar energy generation.[1] At present, the most widely studied, and most efficient, OPVs reported in the literature are bulk heterojunction donor/acceptor blend films of conjugated-polymer donors with fullerene acceptors. The best of these polymer bulk heterojunctions have exhibited power conversion efficiencies of more than 8% under simulated solar conditions.[2,3] The rapid rise in the efficiencies of organic PVs is impressive, yet further gains are necessary to reach commercial viability in many applications, and the ultimate performance limits of OPVs remain an open question of research.[1,4−6]

OPVs are distinct from inorganic photovoltaics in part because OPVs are excitonic devices: due to the low dielectric constants of organic materials, light absorption by an organic semiconductor generates bound electron/hole pairs (excitons) which are subsequently dissociated in a charge transfer event at the donor/acceptor interface. It seems likely that the energy required to dissociate the exciton, and any subsequent recombination losses, will be sensitive to the dielectric constant of the semiconductor layer. Thus, tailoring the dielectric constant of the organic materials has been proposed as a possible route to increase the performance of OPVs.[7]

Both solid-state Graetzel cells[8] and hybrid polymer/quantum dot (QD) blends[9−16] are excitonic solar cells that are closely related to OPVs, but use inorganic acceptors with larger dielectric constants. However, while the higher dielectric constants of inorganic acceptors might prove beneficial in screening Coulombic attraction between the carriers in an excitonic solar cell, the colloidal inorganic materials often have a high density of interfacial surface states, which could lead to carrier trapping. Additionally, because different material combinations disperse differently in bulk heterojunction blends, blending a polymer with phenyl-C_{61}-butyric acid methyl ester (PCBM) can produce different phase separation compared to blending it with colloidal inorganic materials. Furthermore, we expect the electron mobility of the different acceptors to differ, which may also have an effect on the recombination lifetime. These factors suggest that all-organic and hybrid organic/inorganic solar cells may have different efficiency limitations and motivate us to study differences in charge generation and recombination at all-organic and hybrid organic/inorganic interfaces.

In this paper, we present a comprehensive study of the generation and recombination of long-lived charge carriers in a range of donor/acceptor blends utilizing conjugated polymer electron donors and both organic and inorganic electron acceptors. We use quasi-steady-state photoinduced absorption (PIA) spectroscopy to study the dynamics of polymer polarons formed via

Received: August 5, 2011
Revised: October 19, 2011
Published: October 27, 2011

photoinduced electron transfer from three polymers: (1) poly-3-hexylthiophene (P3HT), (2) poly[2-methoxy-5-(3′,7′-dimethyl-octyloxy)-*p*-phenylenevinylene] (MDMO-PPV), and (3) poly-(2,3-bis(2-hexyldecyl)-quinoxaline-5,8-diyl-*alt*-*N*-(2-hexyldecyl)-dithieno[3,2-*b*:2′,3′-*d*]pyrrole) (PDTPQx-HD or PDTPQx). We combine these three polymer donors with a series of acceptors, including the classic soluble fullerene, phenyl-C_{61}-butyric acid methyl ester (PCBM), and inorganic acceptors, including CdSe quantum dots, PbS quantum dots, ZnO nanonetworks, and mesoporous TiO_2 films. We find that, regardless of the polymer, photoinduced electron transfer to all inorganic acceptors yields longer lived polarons and leads to changes in their PIA spectra compared to photoinduced electron transfer to the organic acceptor PCBM. We discuss the increased lifetimes in the context of two explanations and present evidence in support of both: (1) increased charge screening by the higher dielectric constants of the inorganic materials, inhibiting recombination, and (2) charge trapping by surface states on the inorganic materials.

MATERIALS AND METHODS

Cadmium(II) oxide powder (CdO; 99.99+%), selenium powder (Se; ∼100 mesh, 99.99%), trioctylphosphine (TOP), oleic acid (technical grade, 90%), octadecylamine (ODA; 98%), *n*-trioctylphosphine oxide (TOPO; 90%), 1-octadecene (ODE; >95%), hexamethyldisilathiane (HMDS; synthesis grade), ethanedithiol (90+%), and butylamine (>99.5%) were purchased from Sigma-Aldrich. Lead(II) oxide powder (PbO; 99.999+%) was purchased from Strem Chemicals. Pyridine and all organic solvents were purchased from EMD. MDMO-PPV was synthesized in house using a Gilch polymerization route via dehydrohalogenation of appropriate precursors as outlined in the literature.[17] Poly(3-hexylthiophene) (P3HT; M_w = 50 000, rr = 90−93%) was purchased from Rieke Metals. Phenyl-C_{61}-butyric acid methyl ester (PCBM; 99.5%) was purchased from Nano-C.

PDTPQx Synthesis. PDTPQx was synthesized by Stille-type copolymerization of a 2,6-bis(trimethyltin)-*N*-(1-hexyldecyl)-dithieno[3,2-*b*:30-*d*]pyrrole with 5,8-dibromo-2,3-bis(2-hexyldecyl)quinoxaline in anhydrous toluene.[18−22]

Quantum Dot Synthesis. Quantum dot syntheses were all carried out on N_2(g) Schlenk lines using standard air-free techniques.

CdSe quantum dots were synthesized via a modified version of a previously reported hot-injection protocol.[23,24] The cadmium precursor solution was prepared in the following way. A 0.6 mmol portion of CdO and 2 mmol of oleic acid were heated in 2 g of 1-octadecene in a three-neck flask and stirred at 220 °C under N_2(g) flow until the solution became clear, indicating the formation of cadmium oleate. This solution was then cooled to room temperature, at which time 5.5 mmol of ODA and 1.5 mmol of TOPO were added to the mixture, which was then heated to 280 °C. When the solution reached 280 °C, 3 g of SeTOP solution (prepared previously by dissolving 16 mmol of Se powder in 7 g of TOP and 11 g of ODE) was rapidly injected. The reaction temperature was lowered to 260 °C, and the mixture was allowed to react for 5−10 min, at which time it was quenched by submerging the flask in an ice bath. After the reaction mixture was cooled to <70 °C, the quantum dots were extracted with methanol and hexanes several times, and then they were ultimately precipitated with excess methanol and dried under N_2(g).

PbS quantum dots were synthesized via a modified protocol reported by Hines et al.[25] The lead precursor was prepared by stirring 0.6 mmol of PbO with 4 mmol of oleic acid in 14 g of ODE in a three-neck flask under vacuum at 100 °C for at least 1 h. When the solution was clear, the flask was placed under flowing nitrogen gas, and the temperature was raised to 150 °C. Simultaneously, a sulfur precursor solution of 1 mmol of HMDS and 4 g of ODE was prepared in a separate, sealed, three-neck flask under flowing nitrogen gas. The sulfur precursor was rapidly injected into the hot lead precursor and allowed to react for 5−10 min before being quenched in an ice bath. The products were isolated from unreacted precursors and other impurities by precipitation with acetone followed by centrifugation. The resulting precipitate was redispersed in a minimum volume of hexanes and extracted at least three times with methanol. The final products were either precipitated with excess methanol and dried under nitrogen or stored in hexanes in the dark.

Quantum Dot Solution Ligand Exchange. All ligand exchange procedures were carried out in air unless stated otherwise. CdSe quantum dots were treated with pyridine and PbS quantum dots with butylamine.

CdSe quantum dot solutions (in hexanes or chloroform) were transferred to a three-neck flask and dried under N_2(g) flow. N_2(g) was also bubbled through the pyridine. The nitrogen-purged pyridine was added via syringe to the three-neck flask to make a solution of ∼100 mg/mL CdSe quantum dots. The CdSe was stirred and refluxed under N_2(g) for ∼3 h, at which time it was allowed to cool to room temperature and stirred overnight (for at least 12 h). The pyridine solution was removed from the three-neck flask, and the CdSe quantum dots were precipitated into centrifuge tubes with hexanes in air. The solid CdSe precipitate was isolated via centrifugation and dried slightly under N_2(g) flow before being dispersed into chloroform.

Dry PbS quantum dots were removed from the N_2(g) flow and dispersed into nitrogen-purged butylamine with the aid of a sonicater. PbS was dispersed at a concentration of ∼100 mg/mL in butylamine and allowed to sit in solution for several hours. The PbS quantum dots were then precipitated with methanol, dried, and then redispersed into butylamine. After being allowed to sit for another hour, the dots were precipitated with 2-propanol, dried, and dispersed into either chloroform or chlorobenzene.

Film Preparation. Polymer, quantum dot, and blend solutions were spin-coated onto glass microscope slides inside a nitrogen drybox. PIA measurements were carried out in a custom-built chamber that was loaded in the glovebox, sealed, and then attached to a vacuum line for measurements, thus ensuring that the films are not exposed to air at any time during the process. Before measurement, films were stored in the dark under dynamic vacuum for at least 12 h to remove any residual solvent left over from the spin-coating process.

Postdeposition Ligand Treatment of PDTPQx-HD/PbS Films. Ethanedithiol (EDT) solutions were prepared in 20 mL scintillation vials in a nitrogen drybox by adding appropriate amounts of EDT to anhydrous grade acetonitrile. Samples were submerged in the solutions for ∼5 min, at which point they were removed, blown dry with N_2(g), and stored in the dark under dynamic vacuum for at least 12 h before measurement to remove excess EDT and acetonitrile.

Preparation of P3HT/ZnO Films. Nanoscale percolation networks of ZnO were prepared in situ in P3HT films according to literature methods.[26] Briefly, 1.8 mL of 1.1 M diethylzinc in anhydrous toluene was stirred with 3.2 mL of degassed tetrahydrafuran in a nitrogen drybox. This mixture was then mixed with a ∼15 mg/mL solution of P3HT in chlorobenzene at a ratio of 30/70. Samples were spin-coated in air and allowed to stand

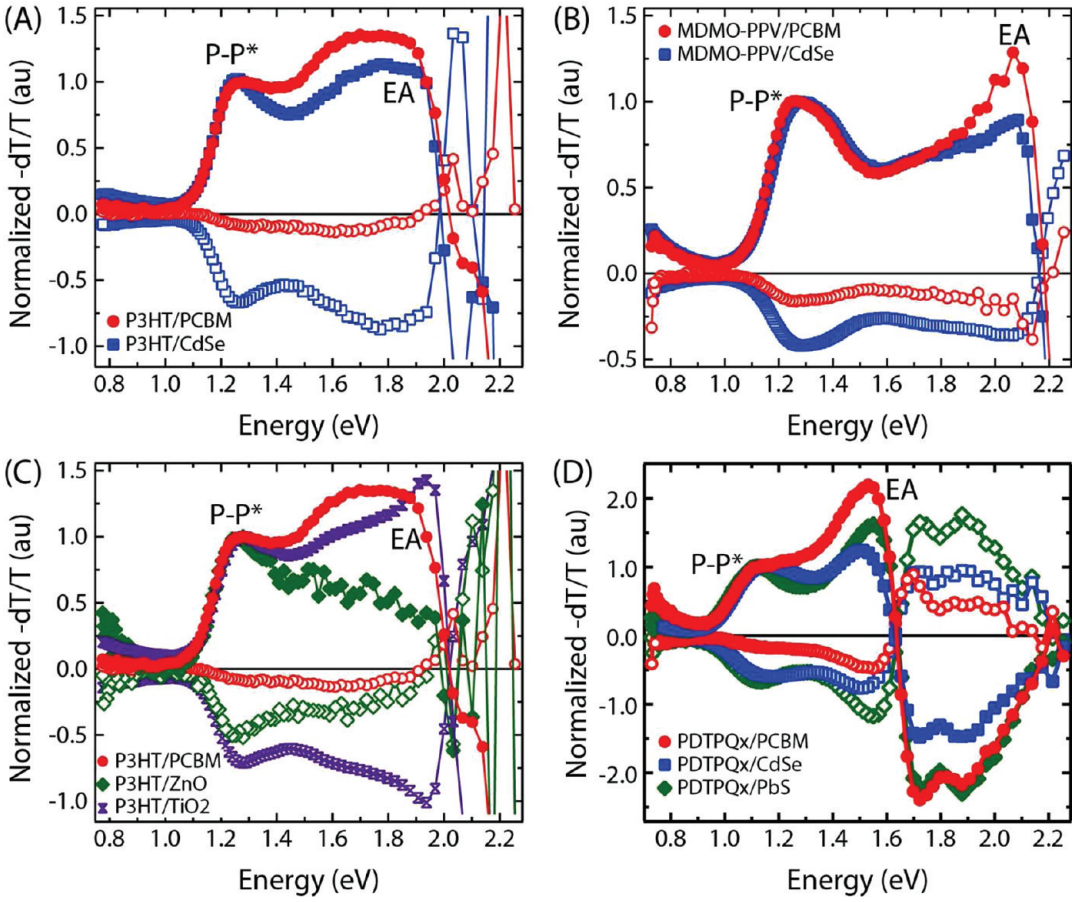

Figure 1. Quasi-steady-state photoinduced absorption spectra for all of the donor−acceptor blends studied in this paper, normalized to the peak of the high-energy positive polaron transition of the polymer donor (labeled P−P*). Filled symbols represent the *x*-channel (in-phase) portion of the signal, and open symbols represent the *y*-channel (out-of-phase) portion. (A) shows the PIA spectra for P3HT/PCBM (red circles) and P3HT/CdSe (blue squares). (B) shows the PIA spectra for MDMO-PPV/PCBM (red circles) and MDMO-PPV/CdSe (blue squares). (C) shows the PIA spectra for P3HT/PCBM (red circles), P3HT/ZnO (green tilted squares), and P3HT/TiO_2 (purple hourglasses). (D) shows the PIA spectra for PDTPQx-HD/PCBM (red circles), PDTPQx-HD/CdSe (blue squares), and PDTPQx-HD/PbS (green tilted squares). All spectra were obtained at room temperature in vacuum, with excitation at 200 Hz modulation frequency by a 700 mW, 455 nm LED.

for 15 min in air with as little light exposure as possible. The samples were then annealed at 100 °C under N_2(g) flow for 15 min prior to being measured.

Preparation of P3HT/Nanoporous TiO_2 Samples. The P3HT/nanoporous TiO_2 films were obtained by first preparing TiO_2 films consisting of nanoparticles ∼18 nm in diameter and then immersing the films in a P3HT solution for adsorption of P3HT molecules. Typically, TiO_2 nanoparticles were synthesized through a hydrothermal method as described elsewhere.[27−29] The as-prepared TiO_2 nanoparticles were made into a thin film with a thickness of ∼10 μm via a doctor-blading method. After a thermal treatment of the films at 450 °C for 30 min to attain a nanoporous structure comprised of nanoparticles interconnected to each other, the films were soaked in a P3HT solution with a concentration of 2 mg/mL in chloroform for 8 h to allow a sufficient adsorption of P3HT molecules on the TiO_2 nanoparticles. The P3HT-adsorbed TiO_2 films were then rinsed with ethanol and dried in air for further use.

PIA Measurements. PIA spectra and frequency dependence were acquired using standard lock-in techniques as discussed in detail elsewhere.[9,11] A 455 nm light-emitting diode (LED; Luxeon Star V, 700 mW, LXHL-LR5C) with a home-built driver circuit was used as the excitation source and was electronically modulated by an Agilent 33120A arbitrary waveform generator. A monochromated tungsten halogen lamp was used as the probe beam, which was detected via a Si/InGaAs dual-band photodetector (Thorlabs, DSD2) with sensitivity from the visible to the near-IR (500−1700 nm). A Stanford Research Systems SR830 lock-in amplifier was used to detect the fractional changes in the probe beam (dT), which are reported normalized to the probe transmission (T) as dT/T values. The phase of the lock-in was set such that scattered LED pump light appeared entirely as a positive signal in the *x*-channel. Thus, a fast absorption induced by the pump appears as a negative dT/T signal in the *x*-channel. Longer lived photoinduced species exhibit more of their overall signal in the out-of-phase detector, denoted as the *y*-channel below. Because the *y*-channel detector is phase lagged by 90° from the *x*-channel detector, the out-of-phase portion of an absorption signal appears as positive in the *y*-channel with the phase set as described above. Corrections were made to subtract any film photoluminescence (PL) or scattered pump light from the PIA spectra by acquired data with the pump beam blocked at each wavelength.

RESULTS AND DISCUSSION

Figure 1 shows the quasi-steady-state PIA spectra for all nine of the donor/acceptor blend combinations studied in this work.

In all cases, filled symbols represent the *x*-channel (in-phase) signal and open symbols represent the *y*-channel (out-of-phase) signal.

Figure 1A shows the PIA spectra for P3HT blended with PCBM (red circles) and with ~3.5 nm CdSe quantum dots (blue squares). Both spectra exhibit the expected P3HT polaron transition at ~1.25 eV (labeled as P−P*),[30] to which they have been normalized to facilitate comparison of spectral shapes across samples of varying thickness and optical density at the pump wavelength. Both spectra also exhibit a broad tail with a second absorption feature peaking at around 1.85 eV (labeled as EA), just to the red of the P3HT highest occupied molecular orbital (HOMO)−lowest unoccupied molecular orbital (LUMO) bleach (the bleach is at the blue end of the spectrum, above 2 eV). The relative intensity of the EA transition is smaller for the P3HT/CdSe sample than for the P3HT/PCBM sample. The second major difference between the PIA spectra for the two different acceptors is the relative magnitude of the *y*-channel (out-of-phase) portion of the signal. In PIA, species with longer lifetimes exhibit larger fractions of their total signal in the out-of-phase channel of the lock-in amplifier. The larger relative *y*-channel to *x*-channel ratio for the P3HT/CdSe blend thus indicates that the average polaron lifetime is longer in the polymer/nanocrystal blend than in the polymer/fullerene blend.

Figure 1B shows PIA spectra for MDMO-PPV blended with PCBM (red circles) and with ~3.5 nm CdSe quantum dots (blue squares). Both spectra exhibit the characteristic MDMO-PPV polaron absorption at ~1.3 eV (labeled as P−P*),[31] to which they have been normalized. As with P3HT, there is a second broad absorption feature to the blue of the polaron transition that peaks just to the red of the bleach of the polymer HOMO−LUMO transition (labeled as EA). In the MDMO-PPV blend the EA transition peaks at ~2.1 eV. Again, as with P3HT, the intensity of the EA relative to the P−P* is *smaller* for the blend with CdSe nanocrystals as acceptors than it is for the blends with the PCBM acceptors. Likewise, blends of MDMO-PPV with CdSe nanocrystals exhibit a larger portion of the polaron signal in the *y*-channel than blends with PCBM, indicating that the average polaron lifetime is longer in the MDMO-PPV/CdSe blends than in the MDMO-PPV/PCBM blends.

To examine if the differences we observed between polymer/PCBM and polymer/CdSe blends were unique to those materials or if the effects were representative of other inorganic acceptors, we conducted PIA experiments on two other systems containing P3HT and inorganic acceptors. Figure 1C shows the PIA spectra for P3HT blended with PCBM (red circles) and with ZnO nanonetworks (green tilted squares) and deposited on top of mesoporous TiO_2 substrates (purple hourglasses). Again, the spectra have been normalized to the P3HT P−P* polaron absorption at ~1.25 eV. The P3HT/ZnO blend again shows a lower relative intensity of the EA absorption than the P3HT/PCBM feature, while the relative intensities of the EA absorption are of comparable size in the P3HT/PCBM and P3HT/TiO_2 blends. The *y*-channel to *x*-channel ratios are larger for the ZnO and TiO_2 blends, again indicative of a longer polaron lifetime in the blends with the inorganic acceptors.

Finally, to examine if the differences between organic and inorganic acceptors observed above extended to other polymer systems beyond the commonly studied P3HT and MDMO-PPV, we conducted PIA on another donor polymer, PDTPQx-HD, which is a derivative (with different side chains) of one of the only donor polymers known to form effective bulk heterojunctions

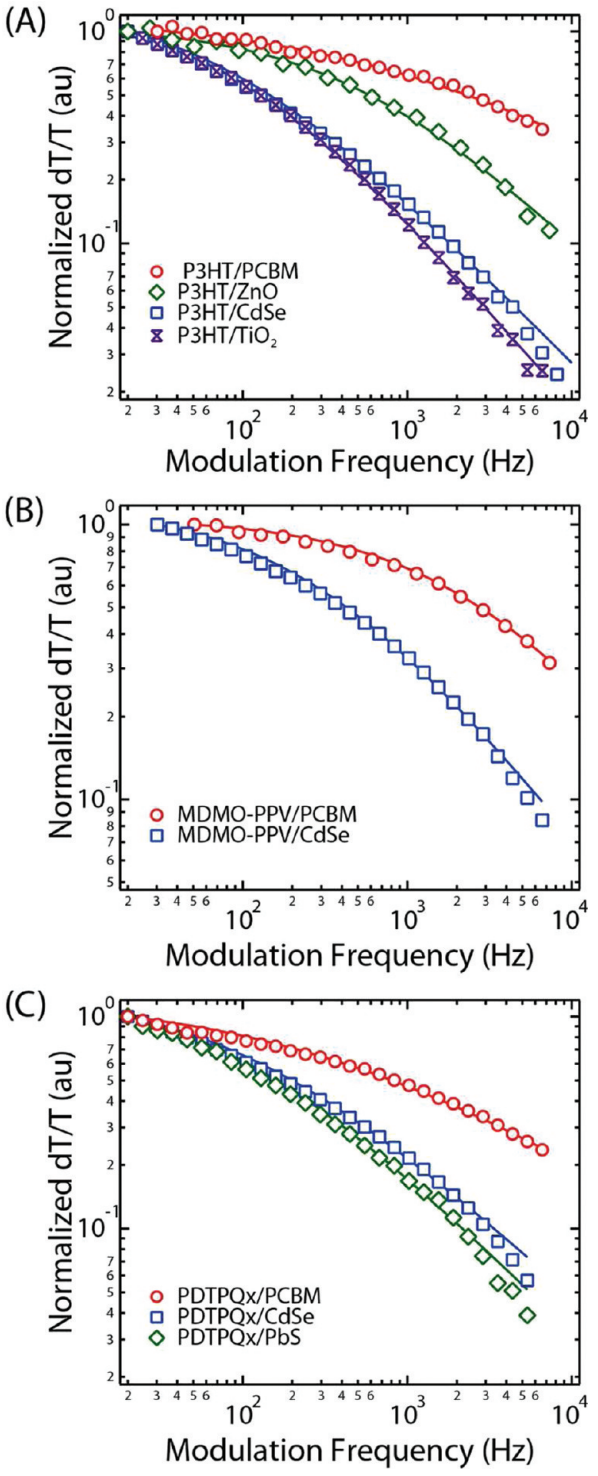

Figure 2. Pump modulation dependence of the PIA signal for each of the donor/acceptor blends studied in this paper. In all cases, the symbols represent data, while the solid lines represent fits to eq 1. (A) shows the modulation dependence of the P3HT P−P* polaron transition at ~1.25 eV for P3HT/PCBM (red circles), P3HT/ZnO (green tilted squares), P3HT/CdSe (blue squares), and P3HT/Ti)$_2$ (purple hourglasses). (B) shows the modulation dependence of the MDMO-PPV P−P* polaron transition at ~1.3 eV for MDMO-PPV/PCBM (red circles) and MDMO-PPV/CdSe (blue squares). (C) shows the modulation dependence of the PDTPQx-HD P−P* polaron transition at ~1.1 eV for PDTPQx-HD/PCBM (red circles), PDTPQx-HD/CdSe (blue squares), and PDTPQx-HD/PbS (green tilted squares).

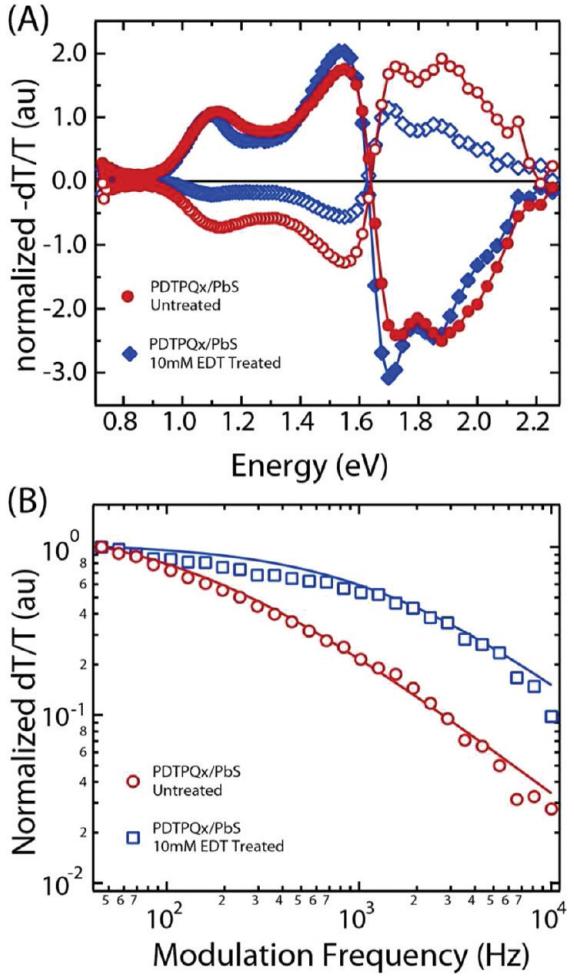

Figure 3. Effect of soaking PDTPQx-HD/PbS blend films in 10 mM EDT on the PDTPQx-HD polaron lifetime. (A) shows the PIA spectra of PDTPQx-HD/PbS blends that were untreated (red circles) and EDT-treated (blue tilted squares), normalized to the PDTPQx-HD polaron transition at 1.1 eV. Closed symbols represent the in-phase (*x*-channel) portion of the spectrum, while open symbols represent the out-of-phase (*y*-channel) portion. (B) shows the modulation dependence of the PIA signal at the PDTPQx-HD polaron transition at ∼1.1 eV for the untreated (red circles) and EDT-treated (blue squares) blends. The symbols represent data, and the solid lines represent fits to eq 1.

with low-band-gap quantum dots such as PbS.[10] Figure 1D shows the PIA spectra for blends of PDTPQx-HD with PCBM (red circles), CdSe quantum dots (blue squares), and ∼3 nm PbS quantum dots (green tilted squares). The spectra have been normalized to the PDTPQx-HD polaron transition at ∼1.1 eV (labeled as P−P*).[10] Once again, there is a second feature just to the red of the polymer HOMO−LUMO bleach between 1.6 and 2.2 eV (labeled EA), and once again, the intensity of the EA feature relative to the P−P* polaron absorption is smaller for both the blends with CdSe and PbS acceptors compared to blends with PCBM. Also, blends of PDTPQx-HD with either of the inorganic acceptors once again exhibit longer lived polarons than blends with PCBM.

The *y*-channel/*x*-channel ratios of the quasi-steady-state PIA spectra provide a qualitative indication that the blends with inorganic acceptors have longer polaron lifetimes. To quantify this observation, we measured the dependence of the PIA signal on

Table 1. Polaron Lifetimes[a] and γ Values for All of the Donor/Acceptor Pairs Discussed in This Work, Resulting from Fitting eq 1 to the Modulation Dependence Data in Figure 2

	acceptor				
polymer	PCBM	CdSe QDs	PbS QDs	ZnO	TiO_2
P3HT	τ = 0.8 ms	τ = 13 ms	n/a	τ = 2 ms	τ = 12 ms
	γ = 0.48	γ = 0.79		γ = 0.75	γ = 0.89
MDMO-PPV	τ = 0.4 ms	τ = 3.5 ms	n/a	n/a	n/a
	γ = 0.74	γ = 0.76			
PDTPQx-HD	τ = 2.2 ms	τ = 10 ms	τ = 7 ms	n/a	n/a
	γ = 0.49	γ = 0.71	γ = 0.86		

[a] Polaron lifetimes are calculated by fitting the total dT/T (R) signal at the peak of the polymer polaron transition vs the pump modulation frequency to eq 1.

the pump modulation frequency. Polarons with lifetimes longer than the inverse of the pump modulation frequency cannot fully decay within the pump's duty cycle, resulting in diminished PIA signal intensity. Thus, longer lived polarons will exhibit a faster falloff with increasing modulation frequency than shorter lived polarons. Modulation dependence data can be fit to a variety of models to determine the kinetics of the measured species. It is often the case that the inhomogeneities of the film and of the energy landscape that charge carriers experience within it produce a variety of scenarios for charge recombination and result in a distribution of lifetimes.[11,32,33] To obtain an average lifetime, we can then fit the total PIA signal, R ($= (X^2 + Y^2)^{1/2}$), with the dispersive recombination equation[33]

$$-\frac{\Delta T}{T} = \frac{\left(\frac{\Delta T}{T}\right)_o}{1 + (\omega\tau)^{\gamma}} \quad (1)$$

where $(\Delta T/T)_o$ is the magnitude of the PIA signal at 0 Hz, ω is the modulation frequency of the pump, τ is the average lifetime, and γ is a factor indicating the degree of dispersity of the lifetimes. Values of γ are less than or equal to 1, with values closer to 1 indicating a narrower distribution of lifetimes.

Figure 2 shows the pump modulation dependence of the PIA signal intensity of the samples from Figure 1. In each case, the probe wavelength was fixed at the wavelength of the polymer P−P* polaron absorption (∼1.25 eV for P3HT, ∼1.3 eV for MDMO-PPV, ∼1.1 eV for PDTPQx-HD). In each plot, the symbols represent experimental data, and the solid lines represent fits to eq 1. The τ and γ values obtained from these fits as well as from fitting modulation dependence data for all of the blends in Figures 1−3 are summarized in Table 1.

Figure 2A shows the modulation dependence of the P3HT P−P* polaron transition at ∼1.25 eV for P3HT/PCBM (red circles), P3HT/ZnO (green tilted squares), P3HT/CdSe (blue squares), and P3HT/TiO_2 (purple hourglasses). Figure 2B shows the modulation dependence of the MDMO-PPV P−P* polaron transition at ∼1.3 eV for MDMO-PPV/PCBM (red circles) and MDMO-PPV/CdSe (blue squares). Figure 2C shows the modulation dependence of the PDTPQx-HD P−P* polaron transition at ∼1.1 eV for PDTPQx-HD/PCBM (red circles), PDTPQx-HD/CdSe (blue squares) and PDTPQx-HD/PbS (green tilted squares). In agreement with the *y*-channel/*x*-channel

ratios in Figure 1, the average lifetimes of long-lived polarons resulting from photoinduced electron transfer from any of the three polymers measured was shorter for blends with PCBM than for blends with the other acceptors. The measured lifetimes are in agreement with previous PIA measurements of P3HT/PCBM,[33] P3HT/TiO_2,[32] MDMO-PPV/PCBM,[34] and PPV/CdSe.[11] In contrast, our measurements of the polaron lifetime for P3HT/CdSe blends are significantly shorter than the 60 ms reported recently,[33] perhaps due to differences in the measurement conditions or materials.

The data presented in Figures 1 and 2 show that, for the nine donor−acceptor blends studied here, polaron lifetimes are always longer when an inorganic material is used as the acceptor as compared to when PCBM is used as the acceptor. There are many possible explanations for these differences. The dispersion of the fullerene in the polymer is likely better than that of the larger inorganic nanoparticles. The materials could exhibit different electron mobilities, which can directly affect recombination times. The inorganic acceptors are likely to possess a much higher abundance of traps due to surface or defect states (which will also affect carrier mobility). Finally, the higher dielectric constants of the inorganic acceptors may help screen long-range Coulombic attractions between carriers in those films. We emphasize that these explanations are not mutually exclusive. However, we focus below on evidence in our experiments that suggests the latter two processes (surface trapping and dielectric screening) are likely to play roles in extending the polaron lifetime.

Deeply bound charge carriers caught in surface traps could exhibit reduced mobility and slower recombination, resulting in longer lived polarons on the polymers. Indeed, Petrozza et al. found that they had to model long-lived, deeply trapped photoinduced electrons in TiO_2 to adequately explain their results from performing charge conductive modulation spectroscopy studies on dye-sensitized solar cells.[35] Additionally, in similar PIA experiments, Heinemann et al.[33] observed longer carrier lifetimes for P3HT/CdSe bulk heterojunction blends vs P3HT/PCBM blends, and they attributed the longer lifetimes to surface traps on the CdSe quantum dot surfaces. Fitting their modulation dependece data to eq 1 yielded lower γ values for P3HT/CdSe and thus more disordered dispersive kinetics, presumably resulting from the trapping and re-release of carriers by the CdSe quantum dots as compared to PCBM. Interestingly, we observe γ values closer to 1 for blends with inorganic acceptors, including CdSe, than for blends with PCBM in all cases except for the MDMO-PPV blends, where the dispersity was essentially identical for both samples. This disparity might be attributed to different measurement conditions as we made our measurements at room temperature on spin-cast samples, corresponding closely to device fabrication and measurement conditions, while Heinemann et al. made theirs at 80 K on drop-cast samples.[33] Additionally, different quantum dot preparation and handling conditions could be expected to yield different distributions of surface trap densities (vide infra). Finally, using transient photocurrent analysis, Li et al.[16] suggested that trapped carriers in P3HT/CdSe blends pose a significant limitation on photovoltaic device efficiency relative to P3HT/PCBM blend devices, which exhibit little trapping behavior. It thus seems likely that traps play some role in extending the lifetimes in all samples, despite the widely different chemistries of the CdSe, PbS, ZnO, and TiO_2 surfaces.

We next consider the hypothesis that the higher dielectric constants of the inorganic acceptors may more effectively screen charge carriers from each other, slowing recombination and thus resulting in the longer observed lifetimes. We propose that the peaks labeled as EA in Figure 1 are electroabsorption features, arising from the Stark effect due to the electric fields associated with the photogenerated carriers in these blends. This assignment is consistent with earlier work by Wei et al. on MEH-PPV (a polymer similar to MDMO-PPV with different side chains). Wei et al. noted that, for MEH-PPV, the feature in question resembles that polymer's electroabsorption spectrum both in its energy and in its derivative shape.[31] As the magnitude of this EA feature is reduced in the blends with CdSe, ZnO, or PbS as compared with PCBM, this assignment would suggest that the average internal electric field is reduced in these samples, presumably due to better screening by the higher effective dielectric constant of the organic/inorganic blends. The one inorganic acceptor that is an exception to this trend is the TiO_2 bilayer film. However, this is also consistent with the dielectric screening hypothesis as the relative difficulty of infiltration of the P3HT into the network film results in a bilayer structure, which would screen electric field propagation throughout the organic layer less effectively than a nanostructured blend with a high-dielectric inorganic semiconductor.

Nevertheless, we acknowledge that the assignment of the exact physical origin of the EA peak has remained difficult over nearly two decades. Recently, Österbacka et al. have assigned the "EA" feature in P3HT blends to delocalized polarons that simultaneously reside on multiple lamellae,[30,33] which form due to the polymer's highly ordered nature in the solid state.[36] However, in our experiments we found that the magnitude of the EA signal was totally unaffected by annealing (section S1 in the Supporting Information), despite the expectation that annealing should promote crystallinity among the P3HT.[37] Furthermore, the observation of an EA feature in widely different polymers argues against interpreting these peaks as delocalized interchain polarons, especially in less-ordered polymers such as MDMO-PPV, which should not support delocalized polarons as well as more crystalline materials such as P3HT.

While the assignment of the peak labled "EA" in Figure 1 to an electroabsorption feature would provide evidence that the average internal electric field in hybrid organic/inorganic blends is reduced from that in polymer/PCBM blends, we have not yet provided direct evidence for the role of surface traps in extending the polaron lifetimes. If trap states are associated with the unpassivated surfaces of the inorganic nanoparticles, then ligand treatments designed to passivate those trap states should mitigate their effect. Previously, Sargent's group demonstrated that thiol treatments could be used to passivate the surfaces of PbS quantum dot solids to decrease the density of deep electron traps, leading to improved carrier mobility and increased device efficiency in Shottky-diode solar cells,[38] and recently Prasad's group has proposed that these benefits extend to bulk heterojunction solar cells,[39] though they did not measure carrier lifetimes or examine charge transfer at the polymer/PbS interface.

To study the effect thiol treatment might have on polymer/QD bulk heterojunction blends, we treated PDTPQx-HD/PbS (50%, w/w) blend films with 1 mM ethanedithiol in acetonitrile for 5 min. Figure 3A shows the PIA spectra for untreated (red circles) and EDT-treated (blue tilted squares) PDTPQx-HD/PbS blends normalized to the PDTPQx-HD polaron transition at 1.1 eV. The filled symbols represent *x*-channel data, and the open symbols represent the *y*-channel data. EDT treatment results in a smaller *y*-channel/*x*-channel ratio and a shorter lifetime.

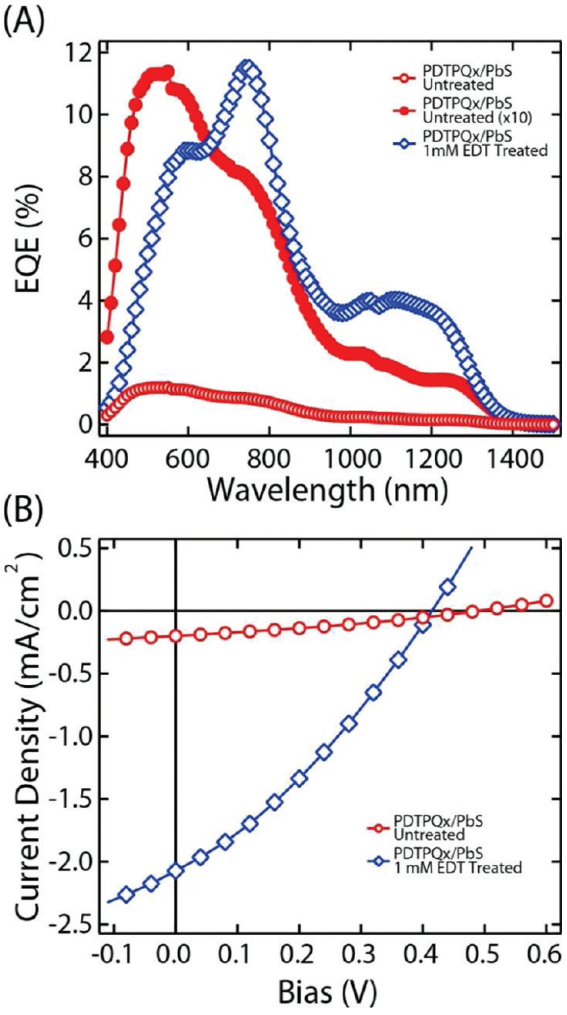

Figure 4. Effect of soaking PDTPQx-HD/PbS active layers in EDT solution on the bulk heterojunction device performance. (A) shows the EQE spectra for untreated PDTPQx-HD/PbS bulk heterojunction blend devices (red circles) and for EDT-soaked PDTPQx-HD/PbS blend devices (blue tilted squares). (B) shows the $I-V$ curves for treated (blue tilted squares) and untreated (red circles) PDTPQx-HD/PbS blend devices collected under AM1.5G simulated solar irradiation.

Figure 3B shows the pump modulation dependence of the PDTPQx-HD polaron absorption at 1.1 eV for the untreated (red circles) and EDT-treated (blue squares) blends. Fits to eq 1, represented in Figure 3B by the solid lines, indicate that the average lifetime decreases from ~7 to ~0.7 ms upon EDT treatment, while the dispersity, γ, was not greatly affected. Since EDT treatment of PDTPQx-HD/PCBM does not greatly affect the polaron lifetime (section S2 in the Supporting Information), we attribute the decrease in lifetime for the PDTPQx-HD/PbS blends to nanocrystal surface passivation by the EDT molecules.

If the decreased lifetimes demonstrated in Figure 3 are, in fact, due to thiols passivating surface traps, we expect to see corresponding improvements in device performance. To test this hypothesis, we fabricated photodiodes with PDTPQx-HD/PbS (90%, w/w) blend active layers and treated them with EDT. Figure 4A shows the external quantum efficiency (EQE) spectra of PDTPQx-HD/PbS films both untreated (open red circles) and treated with 1 mM EDT solution in acetonitrile for 5 min (blue open tilted squares). We also multiplied the untreated spectrum by 10 (solid red circles) to allow comparison of the spectral shapes. Figure 4B shows the $I-V$ curves for untreated (red circles) and EDT-treated (blue tilted squares) PDTPQx-HD/PbS blend devices. This untreated blend had a J_{SC} of 0.17 mA/cm^2, a V_{OC} of 470 mV, a fill factor (FF) of 30.4%, and a power conversion efficiency (PCE) of 0.02%. Treating the blend with EDT decreased the V_{OC} to 404 mV while increasing the J_{SC} to 2.1 mA/cm^2 and the FF to 32.9%, resulting in an overall increase of the PCE by an order of magnitude to 0.25%. The EQE spectra in Figure 4A also change shape upon thiol treatment of the film, possibly due to changes in film morphology, or activation of miniature "Schottky-diode" pathways near the electrodes operating in tandem with the bulk heterojunction.

Nevertheless, the greater than 10-fold increase in short-circuit current upon EDT ligand treatment and the change in polaron lifetime taken together are consistent with the hypothesis that thiols are passivating deep traps on the surface of the quantum dots, resulting in an increased mobility and decreased recombination loss, both of which could improve the efficiency of photogenerated charge collection. While an exhaustive study of the effects of ligand treatment on device performance for all nine donor/acceptor blends is beyond the scope of this work, we believe that surface traps likely contribute to part of the extended lifetimes observed in the polymer/inorganic blends.

CONCLUSION

In summary, we have used photoinduced absorption spectroscopy to study differences in the dynamics of long-lived polarons on three different polymers (P3HT, MDMO-PPV, and PDTPQx-HD) when combined with a range of acceptor materials, both organic (PCBM) and inorganic (CdSe, PbS, ZnO, and TiO_2). For each of the three polymers studied, we measured shorter photoinduced polaron lifetimes when polymers underwent photoinduced charge transfer to the organic acceptor, PCBM, compared to charge transfer to any of the inorganic acceptors. Hybrid polymer/inorganic systems exhibited photoinduced polaron lifetimes up to ~10× longer than those of the polymer/PCBM blends. While our experiments cannot rule out contributions from morphology and intrinsic carrier mobility variations between materials, we found evidence in the form of the diminished electroabsorption features in the PIA spectra of the hybrid blends suggesting that better dielectric screening by the inorganic acceptors is reducing the electric fields felt by the photogenerated carriers in those films. We also found direct evidence for the role of surface states on the performance of organic/inorganic hybrids by the significant changes in both polaron lifetime and device performance that resulted from thiol ligand treatment of PDTPQx-HD/PbS devices.

These results suggest that it may be possible to improve the performance of hybrid organic/inorganic blends to match or even exceed those of the current record-holding all-organic blends if appropriate issues of surface chemistry, film morphology, and processing can be addressed.

ASSOCIATED CONTENT

Supporting Information. UV−vis spectra of P3HT/PCBM blends annealed at different conditions, PIA spectra of P3HT/PCBM blends annealed at different conditions, UV−vis spectra comparing P3HT/PCBM and P3HT/CdSe blends, and PIA spectra and frequency dependence of P3HT/PCBM blends

before and after EDT treatment. This material is available free of charge via the Internet at http://pubs.acs.org.

■ ACKNOWLEDGMENT

This paper is based on work supported primarily by the Department of Energy (Grant DE-FG02-07ER46467). K.M.N. acknowledges partial support from an IGERT Fellowship Award under Grant NSF DGE-050457 at the Center for Nanotechnology at the University of Washington. We thank Lee Y. Park (Williams College) for synthesis of the MDMO-PPV with support from Grant NSF RUI CHE-0415437.

■ REFERENCES

(1) Hoppe, H.; Sariciftci, N. S. *J. Mater. Res.* **2004**, *19*, 1924–1945.
(2) Liang, Y.; Xu, Z.; Xia, J.; Tsai, S.-T.; Wu, Y.; Li, G.; Ray, C.; Yu, L. *Adv. Mater.* **2010**, *22*, E135–E138.
(3) Konarka's Power Plastic Achieves World Record 8.3% Efficiency Certification from National Energy Renewable Laboratory (NREL), 2010. http://www.konarka.com/index.php/site/pressreleasedetail/konarkas_power_plastic_achieves_world_record_83_efficiency_certification_fr.
(4) Noone, K. M.; Ginger, D. S. *ACS Nano* **2009**, *3*, 261–265.
(5) Brabec, C. J.; Sariciftci, N. S.; Hummelen, J. C. *Adv. Funct. Mater.* **2001**, *11*, 15–26.
(6) Chirvase, D.; Parisi, J.; Hummelen, J. C.; Dyakonov, V. *Nanotechnology* **2004**, *15*, 1317–1323.
(7) Servaites, J. D.; Ratner, M. A.; Marks, T. J. *Appl. Phys. Lett.* **2009**, *95*, 163302−1–163302−3.
(8) Ding, I. K.; Melas-Kyriazi, J.; Cevey-Ha, N. L.; Chittibabu, K. G.; Zakeeruddin, S. M.; Gratzel, M.; McGehee, M. D. *Org. Electron.* **2010**, *11*, 1217–1222.
(9) Noone, K. M.; Anderson, N. C.; Horwitz, N. E.; Munro, A. M.; Kulkarni, A. P.; Ginger, D. S. *ACS Nano* **2009**, *3*, 1345–1352.
(10) Noone, K. M.; Strein, E.; Anderson, N. C.; Wu, P.-T.; Jenekhe, S. A.; Ginger, D. S. *Nano Lett.* **2010**, *10*, 2635–2639.
(11) Ginger, D. S.; Greenham, N. C. *Phys. Rev. B* **1999**, *59*, 10622–10629.
(12) Dayal, S.; Kopidakis, N.; Olson, D. C.; Ginley, D. S.; Rumbles, G. *Nano Lett.* **2009**, *10*, 239–242.
(13) Huynh, W. U.; Dittmer, J. J.; Libby, W. C.; Whiting, G. L.; Alivisatos, A. P. *Adv. Funct. Mater.* **2003**, *13*, 73–79.
(14) Milliron, D. J.; Gur, I.; Alivisatos, A. P. *MRS Bull.* **2005**, *30*, 41–44.
(15) Gur, I.; Fromer, N. A.; Chen, C. P.; Kanaras, A. G.; Alivisatos, A. P. *Nano Lett.* **2007**, *7*, 409–414.
(16) Li, Z.; Gao, F.; Greenham, N. C.; McNeill, C. R. *Adv. Funct. Mater.* **2011**, *21*, 1419–1431.
(17) Becker, H.; Spreitzer, H.; Ibrom, K.; Kreuder, W. *Macromolecules* **1999**, *32*, 4925–4932.
(18) Wu, P.-T.; Kim, F. S.; Champion, R. D.; Jenekhe, S. A. *Macromolecules* **2008**, *41*, 7021–7028.
(19) Zhang, X.; Steckler, T. T.; Dasari, R. R.; Ohira, S.; Potscavage, W. J.; Tiwari, S. P.; Coppee, S.; Ellinger, S.; Barlow, S.; Bredas, J. L.; Kippelen, B.; Reynolds, J. R.; Marder, S. R. *J. Mater. Chem.* **2010**, *20*, 123–134.
(20) Ahmed, E.; Subramaniyan, S.; Kim, F. S.; Xin, H.; Jenekhe, S. A. *Macromolecules* **2011**, *44*, 7207–7219.
(21) Subramaniyan, S.; Xin, H.; Kim, F. S.; Shoaee, S.; Durrant, J. R.; Jenekhe, S. A. *Adv. Energy Mater.* **2011**, *1*, 854–860.
(22) Subramaniyan, S.; Xin, H.; Kim, F. S.; Jenekhe, S. A. *Macromolecules* **2011**, *44*, 6245–6248.
(23) Munro, A. M.; Jen-La Plante, I.; Ng, M. S.; Ginger, D. S. *J. Phys. Chem. C* **2007**, *111*, 6220–6227.
(24) Qu, L.; Peng, Z. A.; Peng, X. *Nano Lett.* **2001**, *1*, 333–337.
(25) Hines, M. A.; Scholes, G. D. *Adv. Mater.* **2003**, *15*, 1844–1849.
(26) Oosterhout, S. D.; Wienk, M. M.; van Bavel, S. S.; Thiedmann, R.; Jan Anton Koster, L.; Gilot, J.; Loos, J.; Schmidt, V.; Janssen, R. A. J. *Nat. Mater.* **2009**, *8*, 818–824.
(27) Chou, T. P.; Zhang, Q. F.; Russo, B.; Fryxell, G. E.; Cao, G. Z. *qJ. Phys. Chem. C* **2007**, *111*, 6296.
(28) Ito, S.; Chen, P.; Comte, P.; Nazeeruddin, M. K.; Liska, P.; Pechy, P.; Gratzel, M. *Prog. Photovoltaics* **2007**, *15*, 603–612.
(29) Zhang, Q.; Cao, G. *Nano Today* **2011**, *6*, 91–109.
(30) Osterbacka, R.; An, C. P.; Jiang, X. M.; Vardeny, Z. V. *Science* **2000**, *287*, 839–842.
(31) Wei, X.; Vardeny, Z. V.; Sariciftci, N. S.; Heeger, A. J. *Phys. Rev. B* **1996**, *53*, 2187–2190.
(32) van Hal, P. A.; Christiaans, M. P. T.; Wienk, M. M.; Kroon, J. M.; Janssen, R. A. J. *J. Phys. Chem. B* **1999**, *103*, 4352–4359.
(33) Heinemann, M. D.; von Maydell, K.; Zutz, F.; Kolny-Olesiak, J.; Borchert, H.; Riedel, I.; Parisi, J. *Adv. Funct. Mater.* **2009**, *19*, 3788–3795.
(34) Montanari, I.; Nogueira, A. F.; Nelson, J.; Durrant, J. R.; Winder, C.; Loi, M. A.; Sariciftci, N. S.; Brabec, C. *Appl. Phys. Lett.* **2002**, *81*, 3001–3003.
(35) Petrozza, A.; Groves, C.; Snaith, H. J. *J. Am. Chem. Soc.* **2008**, *130*, 12912–12920.
(36) Kim, Y.; Cook, S.; Tuladhar, S. M.; Choulis, S. A.; Nelson, J.; Durrant, J. R.; Bradley, D. D. C.; Giles, M.; McCulloch, I.; Ha, C. S.; Ree, M. *Nat. Mater.* **2006**, *5*, 197–203.
(37) Giridharagopal, R.; Ginger, D. S. *J. Phys. Chem. Lett.* **2010**, *1*, 1160.
(38) Barkhouse, D. A. R.; Pattantyus-Abraham, A. G.; Levina, L.; Sargent, E. H. *ACS Nano* **2008**, *2*, 2356–2362.
(39) Seo, J.; Cho, M. J.; Lee, D.; Cartwright, A. N.; Prasad, P. N. *Adv. Mater.* **2011**, *23*, 3984–3988.